^{13}CO and $C^{18}O$ observations of S140: delineation of the outflow structure, a study of fractionation effects and comparison with CI observations

Journal Item

Astron. Astrophys. 301, 894–902 (1995)

ASTRONOMY AND ASTROPHYSICS

^{13}CO and $C^{18}O$ observations of S140: delineation of the outflow structure, a study of fractionation effects and comparison with CI observations

Nigel R. Minchin [1], **Glenn J. White** [1] **and Derek Ward-Thompson** [2]

[1] Department of Physics, Queen Mary and Westfield College, University of London, Mile End Road, London E1 3NS, UK
[2] Royal Observatory, Blackford Hill, Edinburgh EH9 3HJ, UK

Received 22 July 1994 / Accepted 2 March 1995

Abstract. The outflow and photon-dominated region (PDR) associated with the S140 complex have been observed at high resolution (~14 arcsec) in the ^{13}CO and $C^{18}O$ J = 3→2 lines. The $C^{18}O$ map confirms earlier $C^{17}O$ J = 3→2 line observations (Minchin et al. 1994) that show an 'arc' of emission observed to the south of the peak, and also reveals a similar (and more prominent) arc feature to the east, a region not covered by the $C^{17}O$ map. This is a particularly fine example of the classic 'tuning fork' morphology, where emission at the ambient cloud velocity is tracing the outflow cavity wall of the blueshifted lobe. The $N(^{13}CO)/N(C^{18}O)$ ratio has been plotted against extinction and fits the power law relation $N(^{13}CO)/N(C^{18}O) = 21A_v^{-0.35}$. The highest values, as expected, occur for observed positions towards the PDR, with $N(^{13}CO)/N(C^{18}O)$ exceeding the terrestrial value (5.5) for $A_v \leq 40$ magnitudes. In the outermost parts of the cloud ($A_v \leq 10$ magnitudes) the $N(^{13}CO)/N(C^{18}O)$ ratio is largest, up to 20. The increased fractionation may be due to higher photoionization of the optically thinner isotope, $C^{18}O$. There is a close correlation between $N(CI)/N(CO)$ and visual extinction over a wide extinction range (A_v=3–100 mags.). The best fit power law is $N(CI)/N(CO)=4.2A_v^{-0.9}$. For positions toward the outflow (A_v~50-100) $N(CI)/N(CO) \sim 0.1$ (0.07-0.12). $N(CI)/N(CO)$ increases with decreasing extinction to ~1 for $A_v \leq 5$ mags., corresponding to positions near the edge of the cloud.

A detailed comparison of antenna temperatures and linewidths for the ^{13}CO, $C^{18}O$ and CI lines is presented. The ^{13}CO and $C^{18}O$ antenna temperatures and linewidths are closely correlated, and imply the emission, for both isotopes, emanates from gas that is in LTE and is well mixed. The CI emission from the PDR implies that here the atomic carbon is in LTE, but occupies a different volume of gas than the isotopic CO. Towards the outflow the CI linewidths are systematically broadened relative to those for the isotopic CO lines. This is interpreted as evidence that atomic carbon is produced by the effect of shocks on the chemical and physical processes at the interface between a stellar wind and the outflow cavity wall.

Key words: ISM: S 140 – ISM: clouds – ISM: atoms – ISM: molecules – jets and outflows – radio lines: ISM

1. Introduction

The S140 complex consists of the L1204 molecular cloud and the S140 HII region, produced by the nearby B0 star HD 211880. The molecular cloud itself consists of an edge-illuminated PDR (e.g. Blair et al. 1978; Evans et al. 1987; White & Padman 1991) and an embedded cluster of three infrared sources (e.g. Beichman et al. 1979) which lie at the centre of a high-velocity molecular outflow (e.g. Snell et al. 1984; Phillips et al. 1988; Minchin et al. 1993 – hereafter Paper I). The blue and redshifted outflow lobes are separated by ~35 arcsec (0.15 pc) in projection, with a high degree of overlap, implying the outflow axis is directed close to the observers line of sight (Paper I). The outflow axis is along the southeast-northwest direction, parallel to the PDR.

Large-scale mapping of the 492 GHz [CI] $^3P_1$–$^3P_0$ line (Keene et al. 1985; Plume et al. 1994) shows emission to be present across the whole of the molecular cloud. Recent high resolution observations of the [CI] $^3P_1$–$^3P_0$ line (~10 arcsec beamwidth) reveal a narrow (~0.1-0.15pc), clumpy, elongated PDR adjacent to the HII region/molecular cloud interface (White & Padman 1991; Minchin et al. 1994 – hereafter Paper II). There is a CI emission peak towards the outflow source and an arc of emission extending from the peak towards the south, which is adjacent to a similar feature observed in $C^{17}O$ J = 3→2 emission (Paper II). This implies the CI emission originates from the inner edge of the blueshifted molecular outflow wall. It is argued that the most plausible mechanism for producing the CI emission from the outflow region is the effect of

Send offprint requests to: Nigel R. Minchin

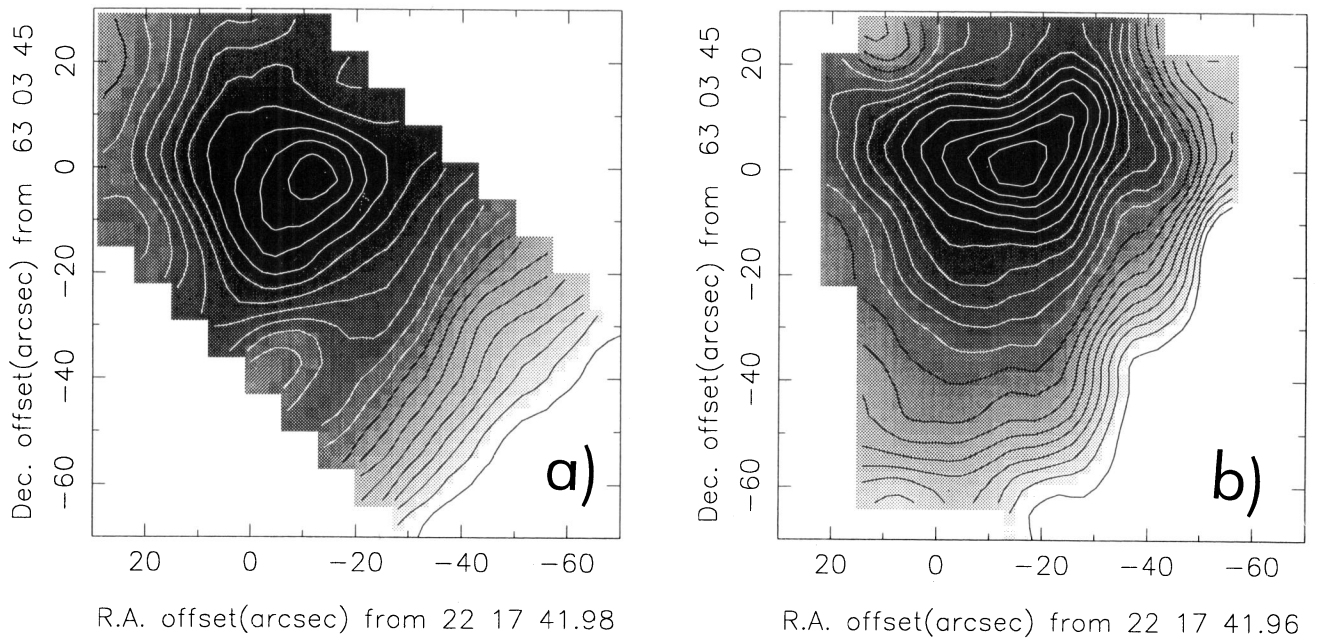

Fig. 1a and b. Greyscale images, with isophotal contour overlayed, of the total integrated intensity between -14 and 2 km s^{-1} for **a** The ^{13}CO J = 3→2 line. The base level contour is 13.2 K-km s^{-1} (3σ) and the contour interval is 1.5σ. **b** The C^{18}O J = 3→2 line. The base level contour is 6 K-km s^{-1} (3σ) and the contour interval is 1σ

shocks on the physical and chemical state at the interface between the stellar wind and the blueshifted outflow cavity wall (e.g. Hollenbach & McKee 1989).

The outline of the paper is as follows. The observations are presented in Sect. 3. They are compared with other recent high resolution molecular and atomic line maps of this region and the implications for the morphology of the region are discussed. In Sect. 4 we present a statistical analysis of ^{13}CO/C^{18}O fractionation, the variation in N(CI)/N(CO) and a comparison of CI and isotopic CO physical and excitation properties.

2. Observations

All observations were carried out at the James Clerk Maxwell Telescope[1] (JCMT), located on Mauna Kea, Hawaii and were obtained in 1988 July 28 (^{13}CO J = 3→2) and 1993 June 5 (C^{18}O J = 3→2). The receiver used was B3i (310-380 GHz), a single channel SIS mixer receiver, used in conjunction with an acousto-optical spectrometer (see White 1988) with 2048 channels and a total bandwidth of 500 MHz for a single IF channel. The telescope was operated in position switching mode, with an off-source reference 10 arcmin to the south and the east. Tracking and pointing were consistently of-the-order 1 arcsec.

The centre position (0,0) for each of the maps is $\alpha_{1950} = 22^h\ 17^m\ 42^s$, $\delta_{1950} = 63^o\ 3'\ 45''$, the position of peak CO emission for the S140 molecular cloud (Paper I). The ^{13}CO J = 3→2 line map consists of 75 spectra taken on a 15×5 grid with the position angle of the y-axis at –45° east of north. The grid spacing is 10 arcsec. The C^{18}O J = 3→2 line map consists of 73 spectra obtained on a standard 14 arcsec grid (14 arcsec is the beam-size at this frequency), with extra spectra obtained at half-beam specing towards the outflow and PDR.

The line observations presented in this paper have been calibrated in units of corrected main-beam brightness temperature T_{mb} (= T_A^*/η_{mb}) and as such have been corrected for all atmospheric, ohmic, scattering and spillover losses. The values of η_{mb} were derived using observations of Mars obtained during the relevent observing run.

3. Results

Figure 1 shows greyscale images of the total integrated intensity between -14 and 2 km s^{-1} for the ^{13}CO and C^{18}O J = 3→2 lines. The morphology delineated by the two maps is similar. The emission is strongly peaked towards the molecular outflow, with extended features towards the northeast, northwest and southwest. The position of the C^{18}O emission peak is offset from the (0,0) position (the position of the ^{12}CO emission peak – see Fig. 3 of Paper I) by ~15 arcsec to the West. The same offset was also observed for the C^{17}O J = 3→2 line (see Fig. 5(a) of Paper II). The ^{13}CO emission peak is offset from the (0,0) position by slightly less, ~10 arcsec. The offset of the emission peak towards the western edge of the cloud appears to increase with decreasing optical depth of the isotopic line, implying it is an optical depth effect. There is a sharp drop in the observed ^{13}CO and C^{18}O emission towards the southwestern edge of the cloud, the position of the PDR.

[1] The James Clerk Maxwell Telescope is operated by the Royal Observatory, Edinburgh, on behalf of the Particle Physics and Astronomy Research Council, the Netherlands Organisation for Pure Research, and the National Research Council of Canada.

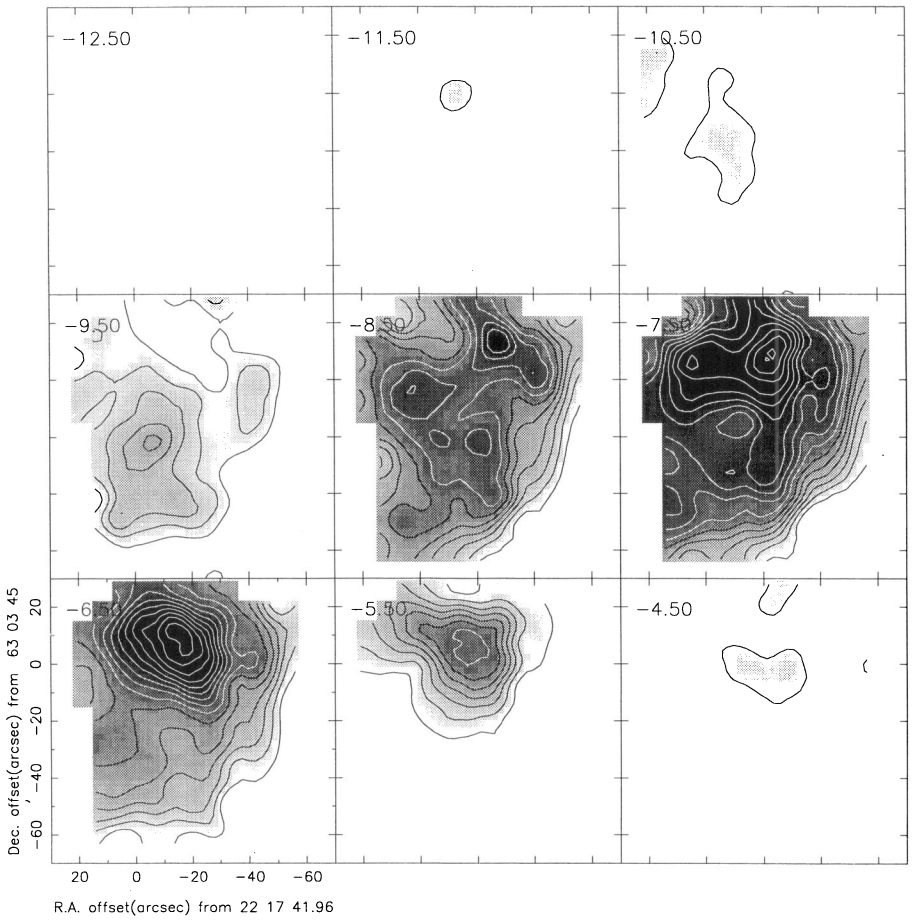

Fig. 2. Velocity channel maps of the $C^{18}O$ J = 3→2 line integrated intensity. Each map is a greyscale image, with isophotal contours overlayed. The channel width is 1 km s^{-1}, with the central velocity of the channel indicated in the top left-hand corner of each map. The base level contour is 1.5 K-km s^{-1} (3σ) and the contour interval is 1σ

Velocity channel maps of the $C^{18}O$ J = 3→2 line are shown in Fig. 2. Note that the channel width and velocity range covered is exactly the same as for the CI and $C^{17}O$ lines shown in Figs. 4 and 6 of Paper II. The $C^{18}O$ and $C^{17}O$ channel maps compare closely, even though the $C^{18}O$ emission is observed over a wider velocity range, due to higher line optical depth. The -8 to -7 km s^{-1} channel (the ambient velocity of the cloud) confirms the $C^{17}O$ 'arc' of emission observed to the south of the peak, but also shows there to be a similar (and more prominent) arc feature to the east (this region was not covered by the $C^{17}O$ map). This is a particularly fine example of the classic 'tuning fork' morphology observed from other outflows (e.g. L1551; Uchida et al. 1987). Here emission at the ambient cloud velocity is tracing the outflow cavity wall of the blueshifted lobe. The outflow wind interacts with ambient cloud material, which accumulates and the density increases accordingly. The position of peak emission in the -11 to -10 and -10 to -9 km s^{-1} channels (blueshifted) is clearly inside of, and bounded by the cavity walls, further confirming the above mentioned scenario.

Greyscale images of the $C^{18}O$ integrated intensity within broad velocity channels are shown in Fig. 3. These cover the blueshifted, core and redshifted emission and use identical velocity ranges as the equivalent maps of the $C^{17}O$ line, shown in Fig. 5 of Paper II. The blueshifted channel (-20 to -10 km s^{-1}) confirms the structure observed in $C^{17}O$ emission, but the larger mapped area of the $C^{18}O$ observations reveal that the 'arc' is actually part of a 'bubble' structure. The diameter of the bubble is ~25 arcsec (~0.1 pc). There are three main emission peaks that delineate the edge of the bubble, centred at (0, -3), (-16, -2) and (-18, -13) respectively. The core channel (-10 to -5 km s^{-1}) shows emission from the ambient cloud, with the peak towards the outflow and extending towards the southwestern edge of the cloud, where it decreases sharply. The red channel (-5 to 5 km s^{-1}) has very little emission, only showing a few low level features, in agreement with the $C^{17}O$ observations; although at the northern edge of the mapped region is the bottom edge of a feature that mat correspond to part of the cavity wall for the redshifted outflow lobe. Further observations of the northern part of the outflow are needed to confirm this feature.

4. Discussion

4.1. $^{13}CO/C^{18}O$ fractionation

To test whether the column densities inferred from CO isotopomeric data are consistent and reliable tracers of N(CO), we have used our $C^{18}O$ and ^{13}CO J = 3→2 line data to derive N(CO). The equations used are derived from the general equation for column density (see Eq. 5 of Paper I) and, for the J = 3→2 lines, are

$$N(C^{18}O) = \frac{T_{ex}}{e^{-31.6/T_{ex}}} 5.14 \times 10^{12} \int T_{mb}(C^{18}O)\, dv \qquad (1)$$

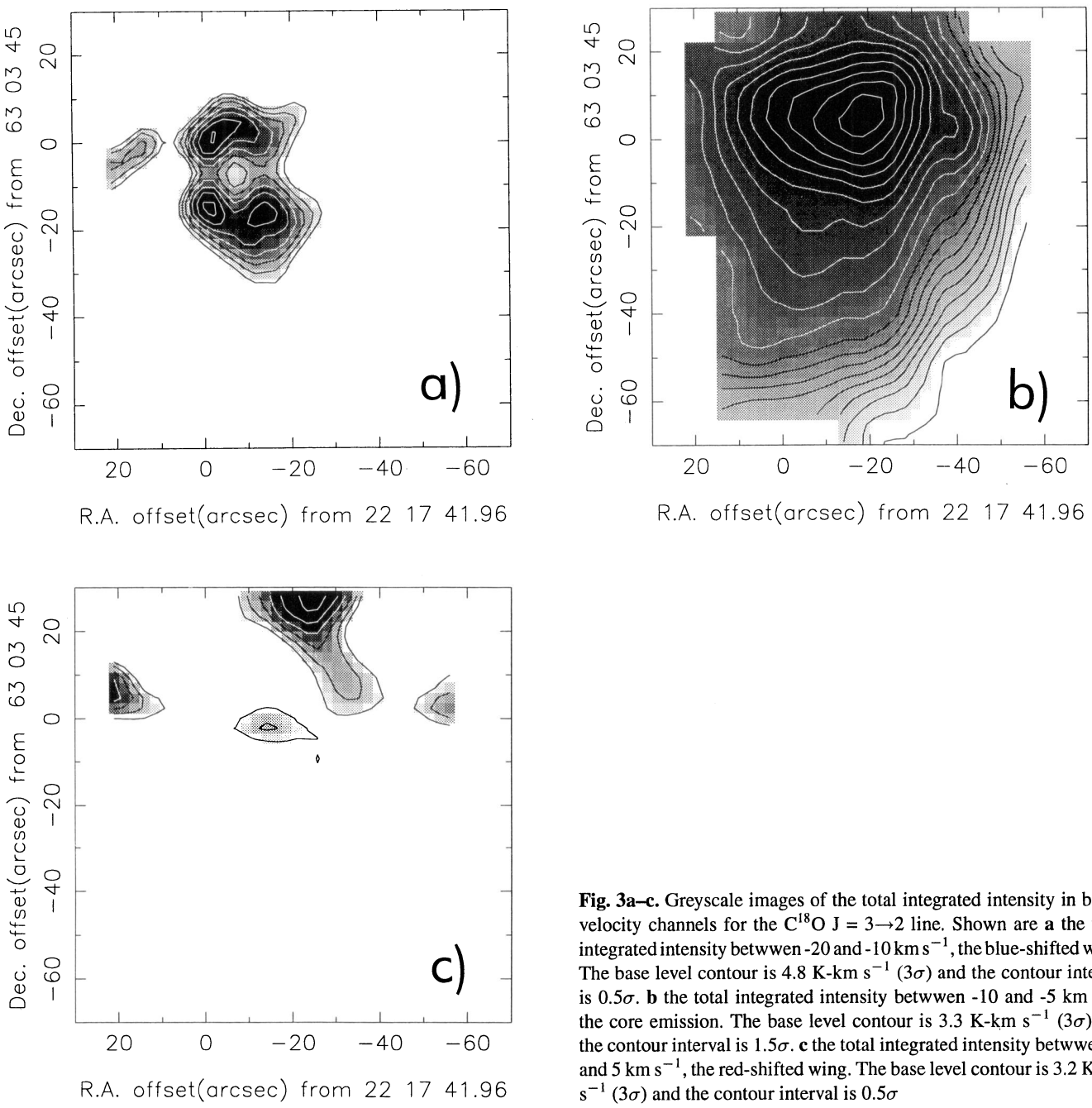

Fig. 3a–c. Greyscale images of the total integrated intensity in broad velocity channels for the C^{18}O J = 3→2 line. Shown are **a** the total integrated intensity betwwen -20 and -10 km s^{-1}, the blue-shifted wing. The base level contour is 4.8 K-km s^{-1} (3σ) and the contour interval is 0.5σ. **b** the total integrated intensity betwwen -10 and -5 km s^{-1}, the core emission. The base level contour is 3.3 K-km s^{-1} (3σ) and the contour interval is 1.5σ. **c** the total integrated intensity betwwen -5 and 5 km s^{-1}, the red-shifted wing. The base level contour is 3.2 K-km s^{-1} (3σ) and the contour interval is 0.5σ

$$N(^{13}\mathrm{CO}) = \frac{T_{\mathrm{ex}}}{e^{-31.7/T_{\mathrm{ex}}}}\, 5.09 \times 10^{12} \int T_{\mathrm{mb}}(^{13}\mathrm{CO})\, dv \qquad (2)$$

Both isotopomers are assumed to have the same excitation temperature, taken to be 50K, a value commonly assumed for this region and consistent with recent derivations (e.g. Paper I). The excitation temperature is unlikely to vary by more than 10-20K from the assumed value, which would only change the derived column density by only 5–10%. The canonical abundances of ^{13}CO and C^{18}O relative to ^{12}CO are assumed to be 70 and 500 respectively (e.g. Langer & Penzias 1990; Gierens et al. 1992). We have applied the correction factor $\beta = \tau/(1 - \mathrm{e}^{-\tau})$, where τ is the line optical depth and is derived from the equation

$$T_{\mathrm{mb}} = \frac{h\nu}{k} \frac{1}{e^{h\nu/kT_{\mathrm{ex}}} - 1} (1 - e^{-\tau}) \qquad (3)$$

using our assumed value of T_{ex} and the observed peak main beam brightness temperature.

As mentioned in Sect. 2, the observing grids used for the ^{13}CO and C^{18}O observations were different. This, coupled with the fact that the CI observations presented in Paper II are at higher resolution (10 arcsec) and were obtained using a smaller-scale grid (5 arcsec), makes comparison of the results difficult. Our solution is to interpolate the ^{13}CO, C^{18}O and CI data and

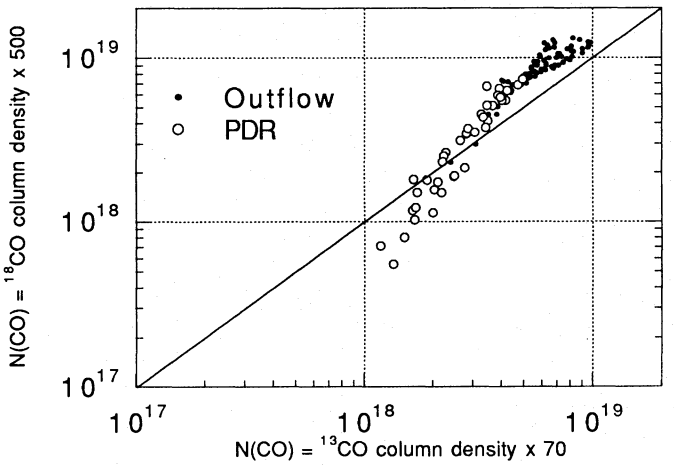

Fig. 4. Comparison of N(CO) derived from the C^{18}O and ^{13}CO column densities multiplied by the canonical abundances relative to CO, assumed to be 70 and 500 respectively. Data points are shown for positions towards the bipolar outflow and PDR. A line is plotted that shows the expected fit if both isotopomers trace the same value of N(CO)

derive the integrated intensity (and thus the column density) at positions on a 5 arcsec spaced grid where data for all three lines were obtained.

Figure 4 shows a plot of N(CO) derived from the C^{18}O data against that derived from the ^{13}CO data. Clearly the level of agreement in N(CO) estimates derived from the two isotopes varies depending on the column density regime. For the positions towards the outflow (N(CO) range 4×10^{18}–10^{19} cm^{-2}) the CO column densities derived from the ^{13}CO and C^{18}O data differ by factors of ~1-5–2, with C^{18}O being overabundant or ^{13}CO underabundant. Towards the PDR ^{13}CO is slightly underabundant relative to C^{18}O at the highest densities (N(CO) range 3×10^{18} – 5×10^{18} cm^{-2}), but overabundant at the lowest densities (N(CO) range 1×10^{18} – 3×10^{18} cm^{-2}), by a factor of ~1.5–2.

This lack of agreement between the column densities derived from different isotopomers could be due to several factors. The higher optical depth of the ^{13}CO line may lead to it being optically thick in the densest regions, whilst the C^{18}O remains optically thin. Although we have made an optical depth correction, this will become increasingly inadequate at high optical depths. Following the same arguement, the lower optical depth of the C^{18}O line implies that it samples material deeper embedded into the cloud/clumps than ^{13}CO lines and thus higher column densities.

Towards the PDR, where the column density is almost an order of magnitude lower and the external UV field is highest (~150G$_o$), the overabundance of ^{13}CO cannot be an optical depth effect. Instead selective photodissociation and enhanced ^{13}CO abundance due to ion-molecule exchange reactions have been used to explain the overabundance of ^{13}CO at the irradiated edges of molecular clouds (e.g. van Dishoeck & Black 1988; Turner et al. 1992). The photodissociation rates for isotopic species are larger than for ^{12}CO at the edges of clouds, owing to smaller self-shielding of the less abundant isotopes. As ^{13}CO is more abundant than C^{18}O it will benefit from greater self-shielding. As the isotopic lines are sufficiently shifted in frequency from those of ^{12}CO, mutual shielding will not be significant. The ^{13}CO abundance is also enhanced due to ion-molecule exchange reactions, in particular

$$^{13}C^+ + ^{12}CO \rightleftharpoons ^{12}C^+ + ^{13}CO + 36K \quad (4)$$

which will significantly enhance the ^{13}CO/C^{18}O ratio at low temperatures (≤40K).

The ratio $N(^{13}CO)/N(C^{18}O)$ has been shown to significantly exceed the terrestrial ratio at the edges of several dark clouds (e.g Frerking et al. 1982; Bachiller & Cernicharo 1986; Lada et al. 1994). Lada et al. (1994) have carried out an extensive study of the dark ckoud IC 5146. They derive extinction estimates using near-infrared colour excess measurements (previous studies used star counts) and mapped the ^{13}CO and C^{18}O J = 1→0 emssion in a 100 arcsec FWHM beam. This work measured extinctions to A_v=15 mags., a significant advance over earlier optical studies.

Using the relationship between N(C^{18}O) and A_v derived by Lada *et al.*, we have plotted $N(^{13}CO)/N(C^{18}O)$ against extinction for the S140 outflow and PDR regions. This is shown in Fig. 5. It should be noted that the Lada et al. relationship was only derived for $A_v \leq 15$ mags., so our extrapolation to higher values may lead to slight inaccuracies, although this will not affect our conclusions. It should also be noted that this analysis implicitly assumes that the observed line-of-sight column density (and hence A_v) is in some way correlated with the extinction towards the exciting star. Given the complex geometry of the region this may not be so. The line-of-sight column density is, however, the only useful measure of extinction available to us. The data fits the power law relation $N(^{13}CO)/N(C^{18}O) = 21A_v^{-0.35}$, with a correlation coefficient of 0.9.

The highest values, as expected, occur for observed positions towards the PDR, with $N(^{13}CO)/N(C^{18}O)$ exceeding the terrestrial value (5.5) for $A_v \leq 40$ magnitudes. In the outermost parts of the cloud, $A_v \leq 10$ magnitudes the $N(^{13}CO)$ to $N(C^{18}O)$ ratio is largest, up to 20. This was also noted in the dark cloud studies of Frerking et al. (1982), Bachiller & Cernicharo (1986) and Lada et al. (1994). Recently White & Sandell (1994) have carried out a similar study of the IRc2/Bright Bar regions of Orion, also allowing direct comparison of outflow and PDR regions and a large number of data points. They also find significant fractionation effects towards the PDR, with the data fitting the power law relation $N(^{13}CO)/N(C^{18}O) = 80A_v^{-0.6}$, with a correlation coefficient of 0.9. This fit is plotted on Fig. 5. What is immediately apparent when comparing the two data sets is the fact that the $N(^{13}CO)$ to $N(C^{18}O)$ ratio observed towards the Bright Bar is systematically higher than observed towards S140 for the same extinction. This is reflected in the different power law fits, and is as high as a factor of 2.5 at the lowest extinctions ($A_v \leq 5$).

The fact that the Bright Bar has a higher incident UV field (~10^5G$_o$) than S140 (~150G$_o$) suggests the increased fractionation may be due to higher photodissociation of the optically

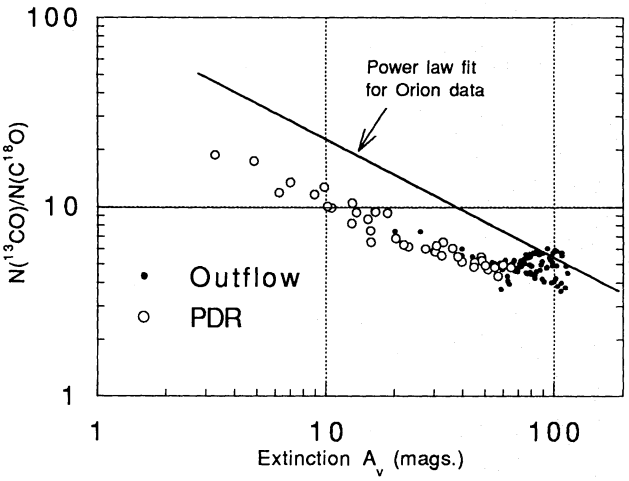

Fig. 5. Graph of $N(^{13}CO)/N(C^{18}O)$ plotted against visual extinction, as estimated from $N(C^{18}O)$. Data points are shown for positions towards the bipolar outflow and PDR. The best fit power law is $N(^{13}CO)/N(C^{18}O) = 21A_v^{-0.35}$, with a correlation coefficient of 0.9

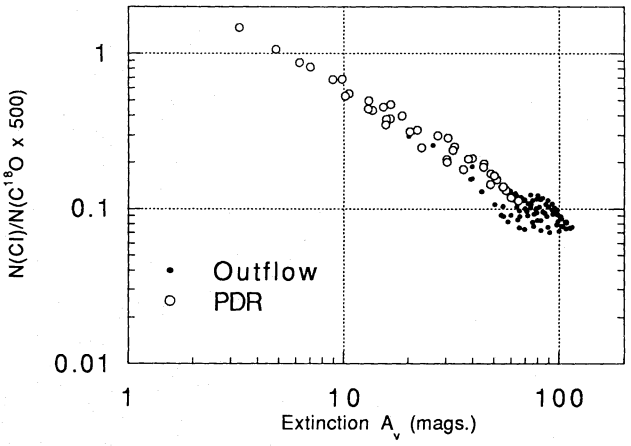

Fig. 6. Graph showing $N(CI)/N(CO)$ plotted against visual extinction, as estimated from $N(C^{18}O)$. $N(CO)$ is derived from $N(C^{18}O)$, assuming a canonical abundance relative to CO of 500. Data points are shown for positions towards the bipolar outflow and PDR. The best fit power law is $N(CI)/N(CO) = 4.2A_v^{-0.9}$, with a correlation coefficient of 1.0

thinner isotope, C^{18}O. This is to be expected as the self-shielding function for each CO isotope is dependent on the isotopic column density, atomic column density, T_{ex} and the external UV field. Current modelling confirms that, for a higher radiation field, C^{18}O is more rapidly dissociated than ^{13}CO at the same A_v. Hence $N(^{13}CO)/N(C^{18}O)$ will be systematically higher (van Dishoeck, private communication). It should also be noted that, as ion-molecule reactions are only efficient at relatively low gas temperatures ($\leq$40K), similar to that found in S140 ($\sim$50K) but much lower than that found in the Orion Bright Bar (up to 200K). Therefore if the $N(^{13}CO)$ to $N(C^{18}O)$ ratio is significantly enhanced by ion-molecule reactions, it would be larger towards S140 than Orion, the opposite of what we observe.

4.2. N(CI)/N(CO) ratio

Figure 6 shows a plot of $N(CI)/N(CO)$ against visual extinction, as estimated from $N(C^{18}O)$. $N(CO)$ is also derived from $N(C^{18}O)$, and assumes a canonical abundance relative to CO of 500. The CI column densities are taken from the [CI] $^3P_1$–$^3P_0$ (492 GHz) data presented in Paper II and have been corrected for optical depth in the same manner as the isotopic CO data, as outlined in Sect. 4.1. The optical depth of the CI line was generally found to be 0.2-0.5 for positions towards both the outflow and PDR and therefore optically thin in both cases. As for the isotopic CO data, an excitation temperature of 50K has been assumed. There has been a great deal of discussion in the literature as to whether it is justifiable to assume the same excitation and chemical conditions for CI as for CO and isotopomers (e.g. Genzel et al. 1988). This will be discussed further in Sect. 4.3. What is clear is that $N(CI)$ is far less sensitive to variations in T_{ex} than CO and isotopomers e.g. doubling $T_{ex}(CI)$ results in changes to $N(CI)\leq 10\%$.

There is a close correlation between $N(CI)/N(CO)$ and visual extinction over a wide extinction range (A_v = 3–100 mags.). The best fit power law is $N(CI)/N(CO) = 4.2A_v^{-0.9}$, with a correlation coefficient of 1.0. This agrees well with the results of White & Sandell (1994) for the Orion IRc2 and Bright Bar regions. They found $N(CI)/N(CO) = 3A_v^{-0.8}$, with a correlation coefficient of 0.8. These results also compare closely with those found for the ρ Ophuichi cloud, over a similar extinction range (Frerking et al. 1989). For positions towards the outflow ($A_v \sim$50-100) $N(CI)/N(CO) \sim 0.1$ (0.07-0.12). $N(CI)/N(CO)$ increases with decreasing extinction to $\sim$1 for $A_v \leq 5$ mags., corresponding to positions near the edge of the cloud. The value of $N(CI)/N(CO) \sim 0.1$ is in close agreement with previous observations of dense regions of molecular clouds, including S140 (e.g. Keene et al. 1985; Zmuidzinas et al. 1988; White & Padman 1991). The high values of $N(CI)/N(CO)$, at low extinction, gives quantitive evidence for the increase in CI abundance in regions of high UV flux, such as edge-illuminated PDRs.

The distribution of $N(CI)/N(CO)$ values with extinction is further evidence for the clumpy nature of molecular clouds. Homogeneous cloud models predict the CI abundance, and hence $N(CI)/N(CO)$, should only be significant in a relatively thin layer ($A_v \sim$3-8 mags.) sandwiched between CII and CO layers (e.g. Tielens & Hollenbach 1985; Hollenbach et al. 1991). This would be observed by $N(CI)/N(CO)$ decreasing rapidly to $\leq$0.1 away from the cloud edge. The gradual decrease in $N(CI)/N(CO)$ with increasing extinction implies UV radiation is able to penetrate deep into the cloud, before dissociating CO. This would be the natural consequence of a clumpy cloud model, where high density clumps are interspersed with a more tenuous interclump medium. This is consistent with the greyscale integrated intensity image of the CI data (Fig. 3a of Paper II), which shows considerable clumpy structure over the mapped region.

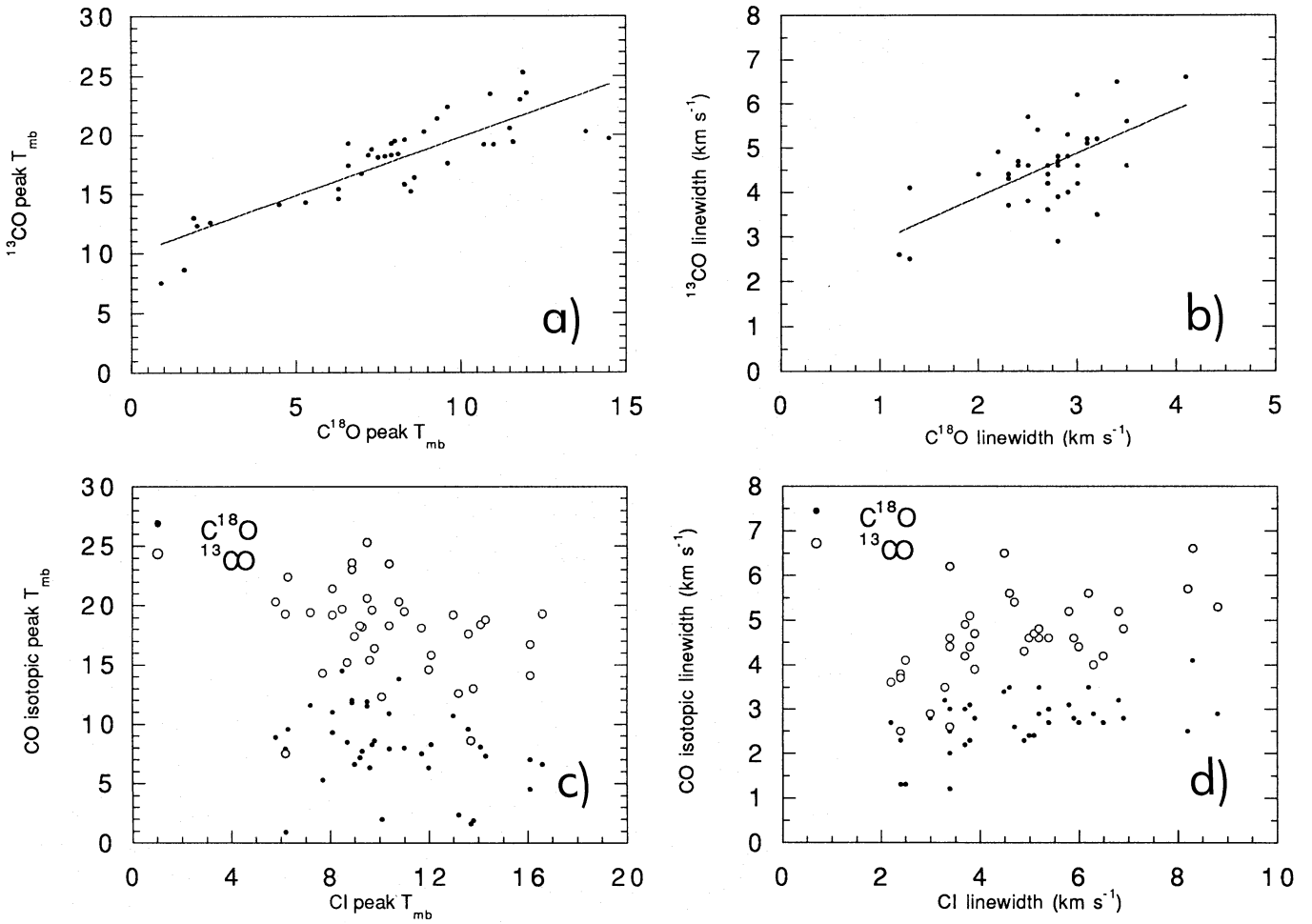

Fig. 7a–d. Graphs showing **a** ^{13}CO peak T_{mb} against C^{18}O peak T_{mb} **b** ^{13}CO linewidth against C^{18}O linewidth **c** Isotopic CO peak T_{mb} against CI peak T_{mb} **d** Isotopic linewidth against CI linewidth

4.3. Comparison of CI and isotopic CO physical and excitation properties

Figure 7 shows various comparisons of ^{13}CO, C^{18}O and CI peak main beam brightness temperatures and linewidths. There is a close correlation between the isotopic CO data for both peak T_{mb} and linewidth (Figs. 7(a) and (b)). The peak T_{mb} values fit the linear relation $T_{mb}(^{13}CO) = 10 + T_{mb}(C^{18}O)$, with a correlation coefficient of 0.8, and the linewidth values fit the linear relation ^{13}CO linewidth = 1.9 + C^{18}O linewidth, with a correlation coefficient of 0.6. This implies isotopic CO linewidths and brightness temperatures increase monotonically with opacity. This had previously been noted for earlier large beam observations (~1 arcmin: e.g. Phillips et al. 1979) and is clearly the case in S140 at the higher resolution of these observations (~14 arcsec).

The close correlation between emission line parameters for the ^{13}CO and C^{18}O lines imply that, even on the smallest observable scales, they are both subject to similar physical and excitation conditions. This is somewhat surprising as the optically thinner isotopic lines (C^{18}O and C^{17}O) appear to trace highly clumpy structure at the highest resolution (e.g. Castets et al. 1991; Dutrey et al. 1993), which is not revealed in ^{13}CO line observations. It is therefore believed that the C^{18}O lines may originate from material deeply embedded in cloud/clump cores, whilst the higher optical depth of the ^{13}CO lines only allow sampling of material from the envelopes of the cloud/clump cores. With the earlier large beam observations one might have expected that any excitation and kinematic variations would not be apparent as the outflow and PDR, separated by only ~70 arcsec, are not resolvable on this scale. The higher resolution observations clearly do resolve the outflow and PDR and thus might have been expected to reveal excitation and kinematic variations for the isotopic lines, considering the differing physical conditions found in the two regions. The simple functional dependence of the linewidth on main beam brightness temperature implies the molecular material is well mixed and in local thermodynamic equilibrium (LTE) over all the density regimes sampled by CO isotopic observations.

The isotopic CO peak T_{mb} and linewidth are plotted against those for the [CI] $^3P_1$–$^3P_0$ line (Figs. 7(c) and (d)). When comparing peak T_{mb} there is no clear relationship present, with the

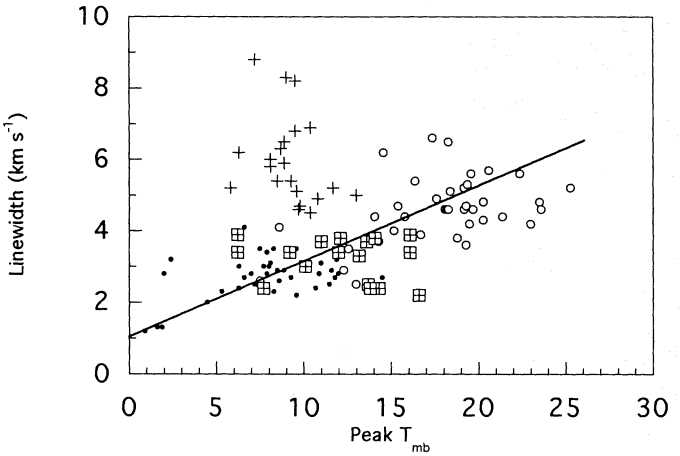

Fig. 8. Graph showing linewidth against peak T_{mb} for the observed lines of ^{13}CO (filled circles), C^{18}O (open circles) and CI outflow (crosses) and PDR (boxed crosses) positions

data points uncorrelated. This is also the case for linewidth, although there is some indication that the isotopic CO and CI linewidths increase together for small CI linewidths, i.e. $\leq$5 km s^{-1}, but are uncorrelated for larger CI linewidths. The same trend is observed for the IRc2 and Bright Bar regions in Orion (White – private communication).

Previous authors have assumed that, for a particular region, the CI lines are formed co-spatially with the CO and that the excitation conditions for CI lines are approximately the same as for CO. The optical depth of CI lines has been estimated from curve-of-growth techniques, assuming that CI linewidths scale with those of CO (e.g. Phillips & Huggins 1981). This was assumed due to the similarity between CO and CI Einstein *A* coefficients and collisional rates. It was also noted that ^{13}CO linewidths and lineshapes closely resembled those of the [CI] $^3P_1$–$^3P_0$ line, although this was based on only a handful of observations. Our high resolution observations provide compelling evidence that line parameters for CI do *not* scale with those of the CO isotopes, implying that either the atomic carbon line emission emanates from a different volume of gas than the isotopic CO emission, or that the atomic material is not in LTE.

Figure 8 shows a plot of peak T_{mb} versus linewidth for the observed ^{13}CO, C^{18}O and CI lines. For both the ^{13}CO and C^{18}O data there is a strong correlation between peak T_{mb} and linewidth, even though ^{13}CO has significantly higher optical depth. The same linear relationship fits both the ^{13}CO and C^{18}O data with linewidth $\sim 1 + 0.2\times T_{mb}$, with the values of peak T_{mb} and linewidth consistently higher for ^{13}CO than C^{18}O. This is consistent with Fig. 7, and confirm that the molecular material is well mixed and in LTE. This is the case for both the outflow and PDR material.

The CI data is split into observed positions towards the outflow (crosses) and PDR (boxed crosses). Towards the PDR the CI data fits the same linear relationship between peak T_{mb} and linewidth as the isotopic CO lines, implying the atomic material is also in LTE. The non-correlation between isotopic CO and CI linewidths and antenna temperatures (Figs. 7(c) and (d)) can therefore be attributed to the isotopic CO and CI emission emanating from different volumes of gas. This conclusion is consistent with the clumpy nature of molecular clouds, which allows UV radiation to penetrate deep into the cloud, photodissociating CO to produce CI at the leading edges of clumps. The observed isotopic CO emission will therefore mainly emanate from the dense, shielded interiors of the clumps, whilst the CI emission is produced on the clump surface.

Towards the outflow, CI linewidths are consistently higher than towards the PDR, $\sim$5-9 km s^{-1}, compared with $\sim$2-5 km s^{-1}. The data does not fit the linear relationship observed for the isotopic CO and the PDR CI observations. This implies a systematic effect is broadening the CI lines emanating from positions towards the molecular outflow. This cannot simply be the effect of the atomic carbon material being entrained within the blue and redshifted outflow, as the isotopic CO lines observed towards the outflow do not show this systematic effect. Instead this is compelling evidence that the CI is produced by the effect of shocks on the chemical and physical processes at the interface between a stellar wind and the outflow cavity wall (e.g. Hollenbach & McKee 1989) as proposed in Paper II. One of the signatures of shocks is the presence of broad emission lines arising from the large dispersion in velocity vectors.

5. Conclusions

The outflow and photon-dominated region (PDR) associated with the S140 complex have been observed at high resolution ($\sim$14 arcsec) in the ^{13}CO and C^{18}O J = 3$\rightarrow$2 lines. The C^{18}O map confirms earlier C^{17}O J = 3$\rightarrow$2 line observations (Minchin et al. 1994) that show an 'arc' of emission observed to the south of the peak, and also reveals a similar (and more prominent) arc feature to the east, a region not covered by the C^{17}O map. This is a particularly fine example of the classic 'tuning fork' morphology, where emission at the ambient cloud velocity is tracing the outflow cavity wall of the blueshifted lobe. The high velocity blueshifted emission is clearly inside of, and bounded by the cavity walls.

The $N(^{13}\mathrm{CO})/N(\mathrm{C}^{18}\mathrm{O})$ ratio has been plotted against extinction and fits the power law relation $N(^{13}\mathrm{CO})/N(\mathrm{C}^{18}\mathrm{O}) = 21\mathrm{A_v}^{-0.35}$. The highest values, as expected, occur for observed positions towards the PDR, with $N(^{13}\mathrm{CO})/N(\mathrm{C}^{18}\mathrm{O})$ exceeding the terrestrial value (5.5) for $\mathrm{A_v}\leq$40 magnitudes. In the outermost parts of the cloud, $\mathrm{A_v}\leq$10 magnitudes the $N(^{13}\mathrm{CO})$ to $N(\mathrm{C}^{18}\mathrm{O})$ ratio is largest, up to 20. The values of $N(^{13}\mathrm{CO})/N(\mathrm{C}^{18}\mathrm{O})$ observed towards the Bright Bar are systematically higher than observed towards S140 for the same extinction. The fact that the Bright Bar has a higher incident UV field ($\sim 10^5 G_o$) than S140 ($\sim 150 G_o$) imply the increased fractionation may be due to higher photoionization of the optically thinner isotope, C^{18}O.

There is a close correlation between $N(\mathrm{CI})/N(\mathrm{CO})$ and visual extinction over a wide extinction range ($\mathrm{A_v}$ = 3–100 mags.). The best fit power law is $N(\mathrm{CI})/N(\mathrm{CO}) = 4.2\mathrm{A_v}^{-0.9}$. For positions towards the outflow ($\mathrm{A_v}\sim$50-100) $N(\mathrm{CI})/N(\mathrm{CO}) \sim 0.1$

(0.07-0.12). $N(CI)/N(CO)$ increases with decreasing extinction to $\sim$1 for $A_v \leq 5$ mags., corresponding to positions near the edge of the cloud. This is interpreted as evidence for the clumpy nature of molecular clouds.

There is a close correlation between the isotopic CO data for both peak T_{mb} and linewidth. This implies isotopic CO linewidths and brightness temperatures increase monotonically with opacity. When comparing CI and CO isotopic data, there is *no* correlation between the observed values of peak T_{mb} and linewidth. A plot of peak T_{mb} versus linewidth for the isotopic CO and CI data implies that towards the PDR the CI data fits the same linear relationship between peak T_{mb} and linewidth as the isotopic CO lines, implying the atomic material is also in LTE. The lack of correlation between isotopic CO and CI linewidths and peak T_{mb} is attributed to the isotopic CO and CI emission emanating from different volumes of gas.

Towards the outflow, CI linewidths are consistently higher than towards the PDR. The data does not fit the linear relationship observed for the isotopic CO observations and the PDR CI observations. This implies that a systematic effect is broadening the CI lines emanating from the molecular outflow. This cannot simply be the effect of the atomic carbon material being entrained within the blue and redshifted outflow, as the isotopic CO lines observed towards the outflow do not show this systematic effect. Instead it is interpreted as evidence that the CI is produced by the effect of shocks on the chemical and physical processes at the interface between a stellar wind and the outflow cavity wall.

Acknowledgements. We wish to thank Juergen Stutzki and Dirk Krause for fruitful discussions on the S140 region and their agreement in using the CI data in this paper. We acknowledge the SERC for travel funds and NRM's PDRA.

References

Bachiller R., Cernicharo J., 1986, A&A 166, 283
Beichman C. A., Becklin E. E., Wynn-Williams C. G., 1979, ApJ Lett 232, L47
Blair G. N., Evans N. J., Vanden Bout P. A, Peters W. L., 1978, ApJ 219, 896
Castets A., Duvert G., Dutrey A. et al., 1990, A&A 234, 469
van Dishoeck E. F., Black J. H., 1988 ApJ 334, 771
Dutrey A., Duvert G., Castets A. et al., 1993, A&A 270, 468
Evans N. J., Kutner M. L., Mundy L. G., 1987, ApJ 323, 145
Frerking M. A., Langer W. D., Wilson R. W., 1982, ApJ 262, 590
Frerking M. A., Keene J., Blake A., Phillips T. G., 1989, ApJ 344, 311
Gierens R., Harris A. I., Jaffe D. T., Stutzki J., 1988, ApJ 332, 1049
Genzel K. M., Stutzki J., Winneswisser G., 1988, A&A 254, 271
Hollenbach D. J., McKee C. F., 1989, ApJ 342, 306
Hollenbach D. J., Takahashi T., Tielens A. G. G. M., 1991, ApJ 377, 192
Lada C. J., Lada E. A., Clemens D. P., Bally J., 1994, ApJ 429, 694
Keene J., Blake A., Phillips T. G., Huggins P. J., Beichman C. A., 1985, ApJ 299, 967
Langer W., Penzias A. A., 1990, ApJ 357, 477
Minchin N. R., White G. J., Padman R., 1993, A&A 277, 595 (Paper I)
Minchin N. R., White G. J., Stutzki J., Krause D., 1994, A&A 291, 250 (Paper II)
Phillips T. G., Knapp G. R., Huggins P. J., Werner etc 1979, ApJ 245, 512
Phillips J. P., et al. 1988, ApJ 190, 289
Phillips T. G., Huggins P. J., 1981, ApJ 251, 533
Plume R., Jaffe D. T., Keene J., 1994, ApJ 425, L29
Snell R. L., Scoville N. Z., Sanders D. B., Erickson N. R., 1984, ApJ 284, 176
Tielens A. G. G. M., Hollenbach D. J., 1985, ApJ 291, 722
Turner B. E., Xu L., Rickard L. J., 1992, ApJ 391, 158
Uchida Y., Kaifu N., Shibata K., Hayashi S. S., Hasegawa T., 1987, In: Star Forming Regions, IAU Symp. No. 115, eds. Peimbert M., Jugka J., Reidel, Dordrecht, p. 287
White G. J., 1988, In: Millimetre and Submillimetre Astronomy, eds. Wolstencroft R. D., Burton W. B., Kluwer, p. 27
White G. J., Padman R., 1991, Nat 354, 511
White G. J., Sandell G., 1994, A&A in press
Zmuidzinas J., Betz A. L., Boreiko R. T., Goldhaber D. M., 1988, ApJ 335, 774

This article was processed by the author using Springer-Verlag LaTeX A&A style file version 3.